

Experimental Investigation of Correlation Properties of MIMO Radio Channels for Indoor Picocell Scenarios

Jean Philippe Kermoal¹, Laurent Schumacher¹, Preben E. Mogensen^{1,2} and Klaus I. Pedersen²

Center for PersonKommunikation¹
Aalborg University, Fr. Bajersvej 7A-5, DK-9220 Aalborg, Denmark
Email: jpk, schum, pm@cpk.auc.dk

Nokia Networks²
Niels Jernesvej 10, DK-9220 Aalborg, Denmark
Email: Klaus.I.Pedersen@nokia.com

Abstract

The present paper describes the set-up for the measurement of MIMO (Multi-Input-Multi-Output) radio channels as part of the European project METRA (Multi Element Transmit and Receive Antenna). Inputs for the stochastic model described in [1] are extracted from the measurement results and fed into a COSSAP[®] block implementing this model. A good matching between the eigenanalysis performed on both measured and simulated signals is shown.

1. Introduction

Extensive work on improving the bit rate to accommodate the increasing demand for throughput in wireless systems by using multi-element transmit and receive antennas has been reported in the literature by Foschini [2] and Andersen [3] among others. The capacity of the Multi-Input-Multi-Output (MIMO) radio channel depends on the spatial correlation properties of the channel. It is important to have a good channel model to obtain realistic results. As an example, preliminary experimental investigations [4] have empirically illustrated for a microcell (Indoor to Outdoor) environment that a total capacity up to 27.9 b/s/Hz can be achieved in the case of a MIMO radio channel using a 4×4 antenna array set-up. As part of the European research project METRA (Multi-Element-Transmit-Receive-Antenna), experimental investigation of the MIMO radio channel for picocell environments is presented in this paper.

A stochastic MIMO model developed by the authors is thoroughly treated in [1]. The present paper is dedicated to the empirical investigation of correlation properties of

MIMO radio channels. The spatial correlation matrix as well as the Doppler power spectrum are extracted from the measurements. They serve as inputs to the stochastic model which main goal is to represent the MIMO radio channel with a single correlation matrix such that not only fully (un)correlated but also partially correlated propagation channels can be investigated. This last option truly reflects real wireless communication scenarios.

The spatial correlation function at the base station (BS) has been well documented in the literature in Lee [5], Adachi et al. [6] for outdoor propagation scenarios along with results in both indoor and outdoor [7]. However, the MIMO channel has not been yet thoroughly experimentally investigated. This lack of expertise motivates the necessity to obtain empirical spatial correlation matrices which provide full information of the spatial correlation between each pair of antenna array element.

In this paper, the measurement set-up, including the used antenna arrays, and the picocell environments are described. MIMO results obtained using a parallel channel sounding measurement testbed are presented. Simulated results produced by the COSSAP[®] implementation of the stochastic MIMO model [8] and measured results of the eigenanalysis are compared and developed in this paper.

2. Measurement Set-up

MIMO measurements with a $M \times N$ set-up, where M and N are the number of elements at the BS and MS respectively, were performed with $M=N=4$. A simplified sketch of the MIMO set-up is presented in Figure 1, where the transmitter (Tx) at the mobile station (MS) is on the left and the stationary receiver (Rx) located at the BS is on the right. The Tx uses a 1-to-4 switch with a switch time of 50 μ s between each element of the antenna array, imple-

menting a pseudo parallel transmission. The BS consists of eight parallel Rx channels, nevertheless due to the configuration set-up only four channels will be considered in this paper. Channel sounding measurements were performed every 20 ms at a carrier frequency of 2.05 GHz (UMTS band) and a chip rate of 4.096 Mcps. A more thorough description of the testbed is given in [9]. The complex narrowband information has been extracted from the wideband channel data.

The MS uses two trolleys. One trolley was carrying all the electronic hardware of the transmitter. The other one, later referred as the “satellite”, was equipped with a linear slide used to move the antenna array at the MS. The two trolleys were connected by 10 m coaxial and signal cables. The purpose of using two trolleys was to avoid any interference from metallic surfaces. The satellite trolley was made of wood and the metallic part of the linear slide was shielded by microwave absorbers. A picture of the MS during one measurement run is shown in Figure 2 where the shield can be seen. The height of the antenna arrays at the MS and the BS were 1.69 m and 2.34 m respectively. The measurements were made free from people moving around to investigate time stationary picocell environments.

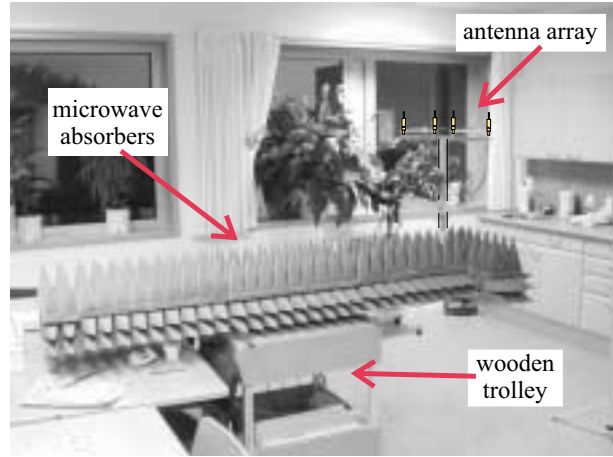


Figure 2. MS “satellite” during a measurement.

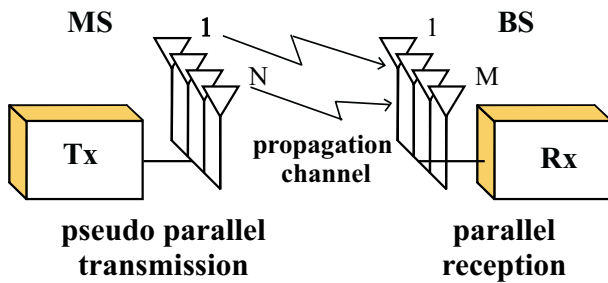


Figure 1. Configuration set-up for parallel channel sounding MIMO measurements.

The MS was moved along the slide over a distance of 9λ , where λ is the wavelength. The measurement procedure is described as follows and illustrated in Figure 3. For a stationary position of the satellite, the antenna array moves forward during 5 s (i.e. from A to B) while the received signals are being recorded. When the array reaches the end of the slide (B) it moves backward while the slide is moved perpendicularly to the motion of the array over a distance of 0.4λ . Starting from C, a new set of measurements is then collected (C to D). This provides two sets of measurements for each MS location. The specific distance of the perpendicular displacement of the slide is later explained in Section 2.1. The acceleration and deceleration phases of the array moving along the slide were disregarded from the measurement analysis.

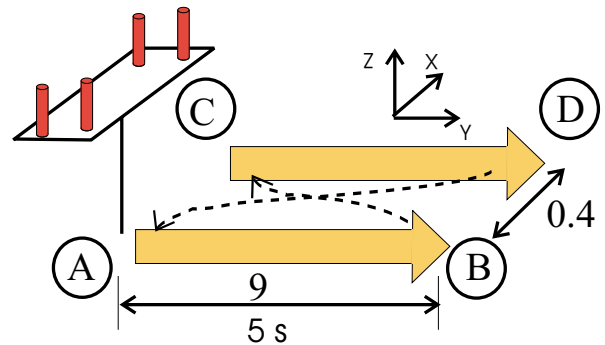


Figure 3. Measurement procedure at the MS.

2.1. Antenna configuration

Vertical polarized sleeve dipoles, with an average return loss of approximately 14 dB and a cross polar discrimination of 20 dB were used during the measurement campaign.

An issue encountered when measuring MIMO radio channels is the mutual coupling between the elements of the antenna array. Figure 4 presents the measured and simulated co-polarized radiation patterns in azimuth of a sleeve dipole when positioned in a 4 element linear array with a separation of 0.5λ . The antenna array was simulated using AWAS©[10], a tool consisting of a kernel for numerical analysis of wire antennas and scatterers. Our confidence in this simulating tool is comforted by the reasonable matching between the measured and the simulated results as illustrated in Figure 4. Clearly the effect of coupling drastically impacts the shape of the radiation pattern since a reduction in gain of 10 dB is noticed for rays coming from 0° or 180° . Such variances in the radiation pattern would directly im-

pact the correlation coefficient (if no postprocessing compensation is made) since the waves coming to the array elements would not be weighted identically. Therefore, in order to measure directly the correlation properties of the MIMO radio channel, it is essential to use array elements with an omnidirectional characteristic. From AWAS ©, different scenarios were investigated to provide an antenna array with an optimum omnidirectional radiation pattern.

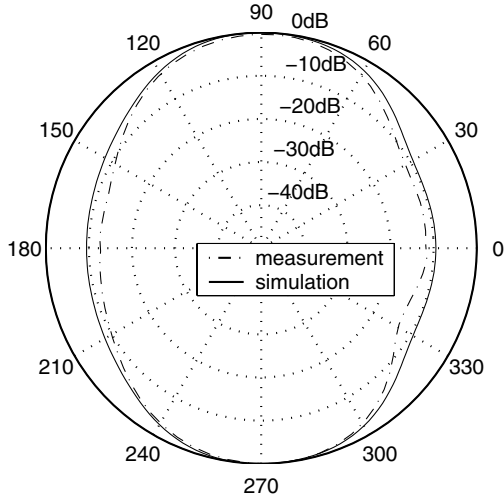


Figure 4. Measured and simulated co-polarized radiation patterns in azimuth of one of the 4 elements of a linear antenna array with 0.5λ separation.

At the MS, an added constraint to the issue of mutual coupling is the separation between the elements of the antenna array to be considered. In order to provide Direction-of-Arrival (DoA) information, it was decided to use 0.4λ separation between the elements to enable to discriminate waves coming from the back from waves coming from the front. Figure 5 presents a sketch of the antenna array used. The interleaved solution provides an actual separation of 1.1λ between the elements compared to a traditional linear array. Furthermore the 3λ separation will both cancel the coupling between the two pairs of elements and create two separate arrays. The x and y axis offset of the array elements is postprocessed to obtain two uniform linear arrays each having four elements separated by 0.4λ . Simulated results of the co-polarization radiation pattern in azimuth for four elements of the antenna array is shown in Figure 6. It can be seen that the influence of the mutual coupling has been sufficiently reduced such that our constraint in terms of omnidirectionality of the radiation pattern is fulfilled.

At the BS, a uniform linear array with four elements and a spacing of 1.5λ was employed since the mutual coupling

influence is low with such a spacing. Moreover, contrary to the MS, no DoA analysis are planned at the BS.

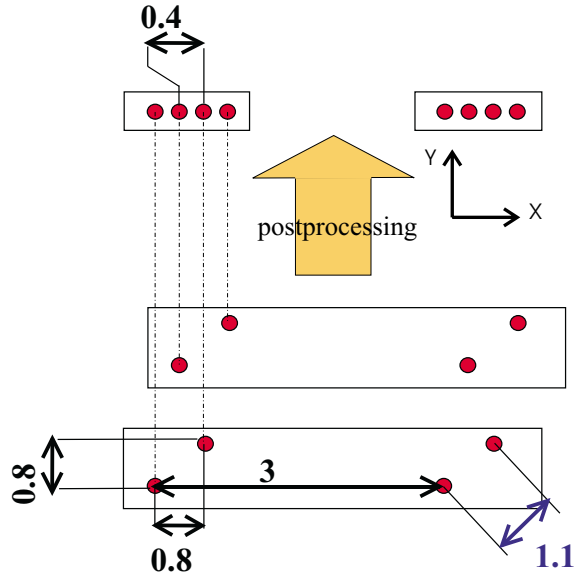


Figure 5. Top view drawing of the antenna array used during the measurement campaign and the postprocessed linear antenna array at the MS.

2.2. Environment

The measurement campaigns were undertaken within several buildings. Three different environments were selected for their different characteristics. The first environment, referred to as Novi2, provides an example of a building with several small offices on the same floor as shown in Figure 7. The second environment, denoted Nokia, illustrates a typical modern open office environment as shown in Figure 8. The last environment, denoted Novi3, is a reception hall. It provides a large open indoor environment with two floors which could easily illustrate a conference hall or a shopping galleria scenario.

For each environment several MS locations were selected to provide a set of measurements where Line-Of-Sight (LOS) and Non-Line-Of-Sight (NLOS) were present. Moreover, several BS locations were selected in addition to the MS locations in order to increase the statistical information of the environment. Table 1 indicates the number of location of the MS and the BS per environment.

The different locations of both the BS and the MS and the layout of the environment are illustrated in Figures 7 and 8. The arrows represent the run of the slide as well as its orientation within the environment. The 4 circles represent

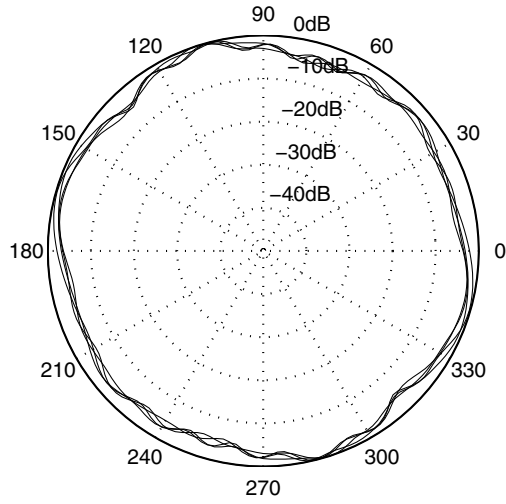


Figure 6. Simulated co-polarized radiation patterns in azimuth of the four elements of the antenna array used during the measurement campaign.

Building identification	Number of BS location	Number of MS location
Novi2	3	7
Novi3	2	9
Nokia	3	5

Table 1. Number of locations of the BS and the MS for each environment.

the linear array for each BS location.

3. Measured and Simulated Results

3.1 Spatial correlation analysis of the MIMO channel

The interest of using MIMO concept is to create parallel subchannels and consequently to increase the capacity of the communication link. It is known from theoretical study [1] that the lower the spatial correlation within the indoor picocell environment, the greater the achieved capacity. One of the goals of the measurement campaign is to evaluate the spatial correlation which exists between several elements of a same antenna array for picocell scenarios.

The complex narrowband information is extracted from

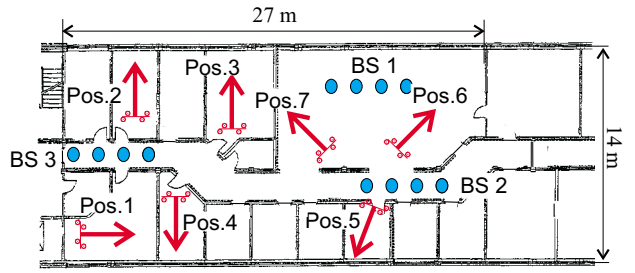


Figure 7. Novi2: layout example of a floor separated by small offices.

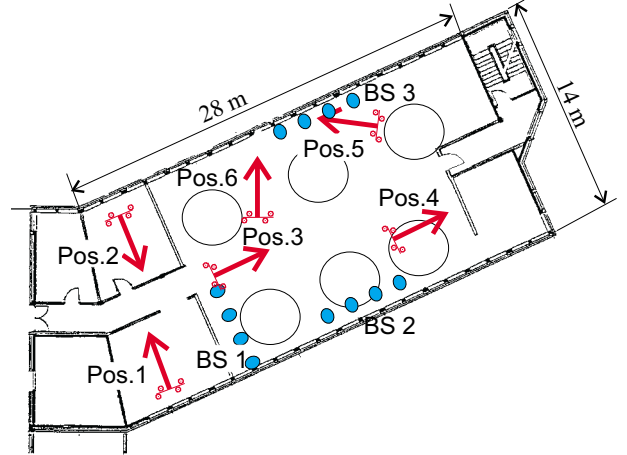


Figure 8. Nokia: layout example of a large open modern office type.

the channel sounding measurement such as

$$h_{mn}(t) = \frac{1}{L} \sum_{l=1}^L h_{mn}(t, \tau_l) \quad (1)$$

where L is the length of the measured complex impulse response $h_{mn}(t, \tau_l)$ associated to its delay τ_l between the m th antenna at the BS and the n th antenna at the MS.

The spatial correlation coefficients $\rho_{m_1 m_2}^{BS}$ and $\rho_{n_1 n_2}^{MS}$ (see Figure 9) defined at both the BS and MS respectively write

$$\rho_{m_1 m_2}^{BS} = \langle |h_{nm_1}|^2, |h_{nm_2}|^2 \rangle \quad (2)$$

$$\rho_{n_1 n_2}^{MS} = \langle |h_{mn_1}|^2, |h_{mn_2}|^2 \rangle \quad (3)$$

The spatial correlation coefficient is defined as

$$\rho = \langle a, b \rangle = \frac{E[ab] - E[a]E[b]}{\sqrt{(E[a^2] - E[a]^2)(E[b^2] - E[b]^2)}} \quad (4)$$

where $E[\cdot]$ denotes expectation. The spatial power correlation coefficient ρ^{power} [11] [12] is derived from (4) by

$$\rho^{power} = |\rho| \quad (5)$$

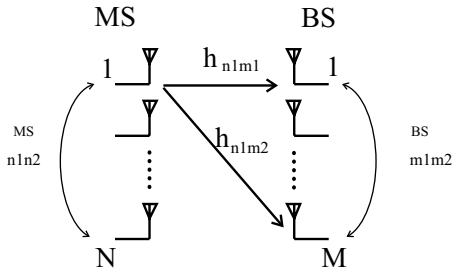


Figure 9. Representation of the spatial correlation coefficients for a MIMO scenario.

The spatial power correlation coefficients at the MS are hereafter analysed. The spatial power correlation coefficient is not treated at the BS since antennas separated with 1.5λ is decorrelated.

Figures 10, 11 and 12 represents the empirical cumulative distribution function (cdf) of the spatial power correlation coefficient computed over all the MS and BS locations for each environment. This means that 21 different locations were considered for Novi2, 12 for Novi3 and 15 for Nokia. For simplicity in reading the graph, the cdf of the spatial correlation between the elements are grouped into three categories with the same spacing (i.e. 0.4λ , 0.8λ and 1.2λ). The curves have to be read such that for instance when looking at Figure 10, at 50 % of the measured location for the environment Novi2, the spatial correlation at the MS for each element separated with 0.4λ is less than 0.3. It can be seen that for the three environments, the elements of the MS are decorrelated.

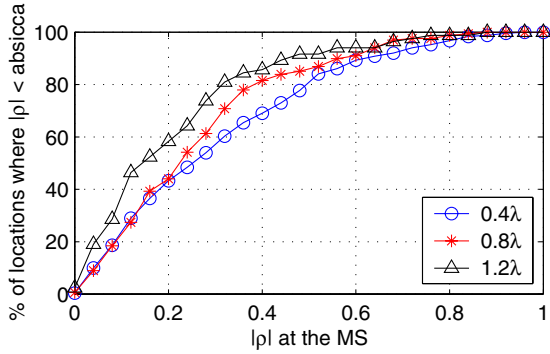


Figure 10. Empirical cdf of the spatial power correlation coefficient for Novi2.

3.2 COSSAP® implementation

Another aim of the measurements is to derive realistic parameters of the MIMO radio channel and to feed them

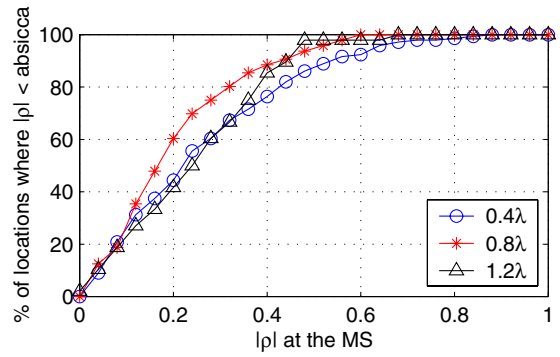


Figure 11. Empirical cdf of the spatial power correlation coefficient for Novi3.

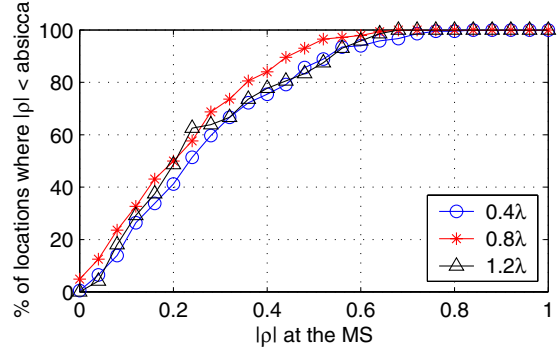


Figure 12. Empirical cdf of the spatial power correlation coefficient for Nokia.

into the COSSAP® implementation of the stochastic channel model described in [1] in order to validate it.

These parameters presented later are extracted from two positions (i.e. pos A and pos B) which reflect two different propagation characteristics. The input parameters given to the COSSAP® MIMO model are the followings:

- The spatial power correlation matrix \mathbf{R}_{MS} at the MS.
- The spatial power correlation matrix \mathbf{R}_{BS} at the BS.
- The Doppler spectrum of the signal.

The correlation matrices \mathbf{R}_{MS} and \mathbf{R}_{BS} are both defined as

$$\mathbf{R}_{BS} = [\rho_{ij}^{BS,power}], i, j \in \{1 \dots M\} \quad (6)$$

$$\mathbf{R}_{MS} = [\rho_{ij}^{MS,power}], i, j \in \{1 \dots N\} \quad (7)$$

where ρ_{ij}^{power} is the spatial correlation defined previously.

The measured power correlation matrices used in the simulations are presented below. They are the result of an average over the reference antennas with respect to which

the measured spatial power correlation matrices are computed.

$$\mathbf{R}_{\text{MS}}^{\text{pos A}} = \begin{bmatrix} 1 & 0.3394 & 0.0856 & 0.1615 \\ 0.3394 & 1 & 0.2947 & 0.1379 \\ 0.0856 & 0.2947 & 1 & 0.2490 \\ 0.1615 & 0.1379 & 0.2490 & 1 \end{bmatrix} \quad (8)$$

$$\mathbf{R}_{\text{BS}}^{\text{pos A}} = \begin{bmatrix} 1 & 0.2628 & 0.2550 & 0.1216 \\ 0.2628 & 1 & 0.2417 & 0.2143 \\ 0.2550 & 0.2417 & 1 & 0.2896 \\ 0.1216 & 0.2143 & 0.2896 & 1 \end{bmatrix} \quad (9)$$

$$\mathbf{R}_{\text{MS}}^{\text{pos B}} = \begin{bmatrix} 1 & 0.6951 & 0.2082 & 0.2404 \\ 0.6951 & 1 & 0.3411 & 0.2603 \\ 0.2082 & 0.3411 & 1 & 0.3253 \\ 0.2404 & 0.2603 & 0.3253 & 1 \end{bmatrix} \quad (10)$$

$$\mathbf{R}_{\text{BS}}^{\text{pos B}} = \begin{bmatrix} 1 & 0.3173 & 0.1781 & 0.1189 \\ 0.3173 & 1 & 0.7603 & 0.5366 \\ 0.1781 & 0.7603 & 1 & 0.7973 \\ 0.1189 & 0.5366 & 0.7973 & 1 \end{bmatrix} \quad (11)$$

The average measured Doppler power spectrum of the MS seen from the BS applied to the channel model is presented in Figures 13 and 14. The Doppler spectra of pos A and pos B, normalized to the maximum Doppler shift f_m , present two different propagation characteristics.

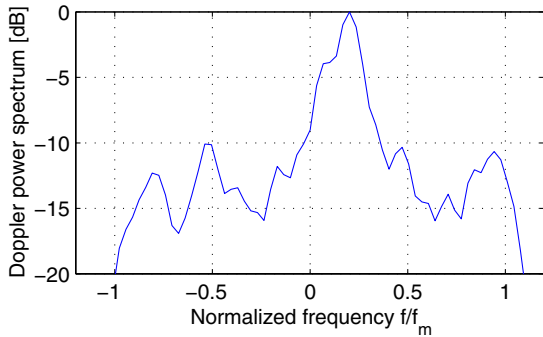


Figure 13. Average empirical Doppler power spectrum for pos A.

In order to check the matching between the measured and simulated results, their eigenanalysis is performed in the following section.

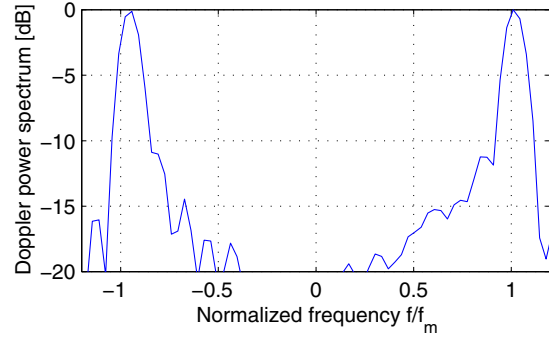


Figure 14. Average empirical Doppler power spectrum for pos B.

3.3 Measured and simulated eigenanalysis results

A method to estimate the number of independent channels between two terminals in a rich scattering environment is to use the eigenvalue decomposition [3] of the instantaneous correlation matrix \mathbf{R} defined as

$$\mathbf{R} = \mathbf{H}\mathbf{H}^H \quad (12)$$

where \mathbf{H} is the narrowband complex channel matrix and $[\cdot]^H$ represents Hermitian transposition. \mathbf{H} is expressed as

$$\mathbf{H} = \begin{bmatrix} h_{11} & h_{12} & \dots & h_{1N} \\ h_{21} & h_{22} & & \\ \vdots & & \ddots & \vdots \\ h_{M1} & & \dots & h_{MN} \end{bmatrix}$$

where h_{mn} is defined in (1).

A channel matrix \mathbf{H} may offer k parallel subchannels with different mean gains, with k defined as

$$k = \text{Rank}\{\mathbf{R}\} \leq \min\{M, N\} \quad (13)$$

where the function $\text{Rank}\{\cdot\}$ and $\min\{\cdot\}$ returns the rank of the matrix argument and the minimum value of the arguments respectively. The k^{th} eigenvalue is to be visualised as the power gain of the k^{th} channel [3]. An investigation of the measured and simulated data in terms of eigenvalues is presented below.

The simulated data sets have been generated according to a two phase procedure.

Phase 1 \mathbf{R}_{MS} and \mathbf{R}_{BS} are mapped to the identity matrix. The measured complex Doppler spectra (i.e. with phase and magnitude information) of the MN paths h_{mn} are fed into the model. This is a first validation of the model with respect to the implementation of the fading.

Phase 2 The true average spatial power correlation matrices \mathbf{R}_{MS} and \mathbf{R}_{BS} are applied to the model. MN i.i.d. variables with amplitude shaped by the average Doppler power spectrum and random phase uniformly distributed over $[0, 2\pi[$ are generated by the model.

The cdf of the channel envelope h_{mn} and the eigenvalues λ_k (not to be confused with the wavelength λ) for a full run of the transmitter along the linear slide is displayed in Figures 15 and 16 for pos A and B respectively. Measured and simulated results are both presented on the same graph. The eigenvalues are normalized to the mean gain value of a single transmit and single receive element h_{mn} of the channel matrix \mathbf{H} . It can be seen that the environment of the two considered cases is decorrelated. This makes the eigenvalues more predominant than in a correlated scenario and consequently parallel subchannels are achieved within the investigated picocell with only 0.4λ separation.

Moreover simulated and empirical cdf's of the channel envelope fit well with the Rayleigh distribution reference line. This shows that for the two cases the channel is almost Rayleigh distributed.

The simulated phase 1 fits perfectly well with the measured cdf in both figures as one would expect. From simulated phase 2, it can be seen that the simulated results are close to the measured ones. They may be several reasons why the simulated and measured results do not match perfectly: insufficient amount of statistics, Wide-Sense Stationary (WSS) assumption not 100% fulfilled, ... This needs further investigations. Nevertheless, it is fair to conclude from the matching of the curves in Figures 15 and 16 that the stochastic channel model is validated.

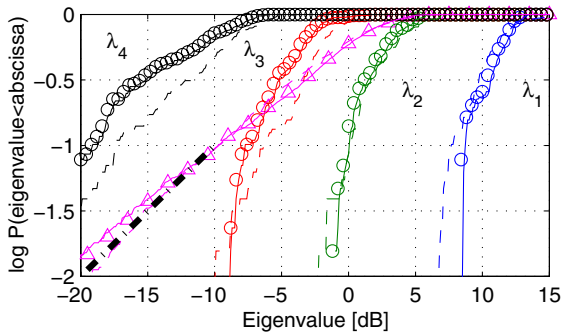


Figure 15. Empirical cdf of narrowband channel envelope and the eigenvalues for pos A (Δ : h_{mn} , \circ : measured λ , continuous line: simulated phase 1, dashed line: simulated phase 2, thick dash-dotted line: Rayleigh distribution reference).

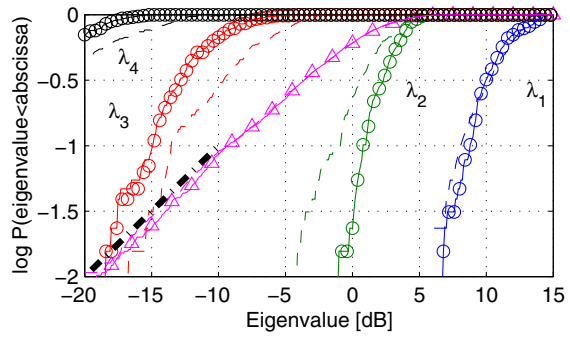


Figure 16. Empirical cdf of narrowband channel envelope and the eigenvalues for pos B (Δ : h_{mn} , \circ : measured λ , continuous line: simulated phase 1, dashed line: simulated phase 2, thick dash-dotted line: Rayleigh distribution reference).

4. Conclusion

This paper presented the set-up and the initial results of measurements of MIMO radio channels performed as part of the European project METRA. Exploitation of the measurements showed that 0.4λ separation between the elements of the antenna array is sufficient to have them decorrelated. Doppler spectra and spatial power correlation matrices were derived from these measurements to serve as inputs of a COSSAP[®] block implementing a stochastic model of the MIMO radio channel. Comparison of the eigenanalyses performed on both measured and simulated signals demonstrated a good matching between the implemented stochastic model and the real measurements.

References

- [1] K. I. Pedersen, J.B. Andersen, J.P. Kermaol, and P. Mogensen, "A Stochastic Multiple-Input-Multiple-Output Radio Channel Model for Evaluation of Space-Time Coding Algorithms", *accepted for IEEE Vehicular Technology Conference VTC 2000 Fall, Boston, USA, 2000*.
- [2] G.J. Foschini, "Layered Space-Time Architecture for Wireless Communication in a Fading Environment When Using Multi-Element Antennas", *Bell Labs Technical Journal*, vol. 1, no. 2, pp. 41–59, Autumn 1996.
- [3] J.B. Andersen, "Array Gain and Capacity for Known Random Channels with Multiple Element Arrays at

Both Ends”, *IEEE Journal Selected Areas in Communications*, to be published.

- [4] J.P. Kermoal, P.E. Mogensen, S.H. Jensen, J. B. Andersen, F. Frederiksen, T. B. Sørensen, and K.I. Pedersen, “Experimental Investigation of Multipath Richness for Multi-Element Transmit and Receive Antenna Arrays”, *IEEE Vehicular Technology Conference VTC 2000 Spring, Tokyo, Japan*, vol. 3, pp. 2004–2008, May 2000.
- [5] W. C. Y. Lee, “Effects on Correlation Between Two Mobile Radio Base-Station Antennas”, *IEEE Transactions on Vehicular Technology*, vol. 22, no. 4, pp. 130–140, November 1973.
- [6] F. Adachi, M.T. Feeney, A.G. Williamson, and J.D. Parsons, “Crosscorrelation Between the Envelopes of 900 MHz Signals Received at a Mobile Radio Base Station Site”, *IEE Proceedings*, vol. 133, Pt. F, no. 6, pp. 506–512, October 1986.
- [7] P.C.F. Eggers, J. Toftgård, and A.M. Oprea, “Antenna Systems for Base Station Diversity in Urban Small and Micro Cells”, *IEEE Journal on Select Areas in Communications*, vol. 11, no. 7, pp. 1046–1057, September 1993.
- [8] L. Schumacher, K.I. Pedersen, J.P. Kermoal, and P. Mogensen, “A Link-Level Simulator Implementing a Stochastic MIMO Radio Channel Model for Evaluation of Space-Time Coding Algorithms”, *accepted for IST Mobile Communication Summit 2000, Galway, Ireland*, 2000.
- [9] F. Frederiksen, P. Mogensen, K.I. Pedersen, and P. Leth-Espensen, “A “Software” Testbed for Performance Evaluation of Adaptive Antennas in FH GSM and Wideband-CDMA”, *Conference Proceeding of the 3rd ACTS Mobile Communication Summit, Rhodes, Greece*, vol. 2, pp. 430–435, June 8-11 1998.
- [10] *AWAS for windows, version 1.0*, Copyright 1995 Artech House, Inc, 1995.
- [11] Jr. W. C. Jakes, *Microwave Mobile Communications*, John Wiley and Sons, Inc, 1974.
- [12] W. C. Y. Lee, *Mobile Communications Engineering*, McGraw-Hill Book Company, 1982.